Regioselectivity in Iron-Catalyzed [2+2+1] Cycloadditions: A DFT Investigation of Substituent Effects in 1,4-Diazabutadienes

Wolfgang Imhof*[a] and Ernst Anders[b]

Dedicated to Prof. Dr. Eckhard Dinjus on the occasion of his 60th birthday

Abstract: The transition-metal-catalyzed [2+2+1] cycloaddition reaction of 1,4-diazabutadienes, in which the imine-carbon atoms are part of an oxazine ring system, with ethylene and carbon monoxide leads to the regioselective formation of pyrrolidinone derivatives. To explain this regioselectivity, the transition states and intermediates of the rate-determining step of the catalysis are determined by high-level DFT calculations. The experimentally observed regioselectivity is consistent with the lower activation energy of the addition of ethylene towards the carbon atom next to the oxazine oxygen atom. Furthermore, the activation barrier of a conceivable back reaction is higher for the intermediates with the experimentally observed regioselectivity. These thermodynamic and kinetic arguments at first sight appear to be confirmed by the calculated NPA charges in the transition states, which reveal that the differences in these charges are greatest for those transition states that lead to the formation of the energetically favored transition structures. Nevertheless, calculations of analogous transition structures and reaction products starting from 1,4-diazabutadienes with a 2-fluoro, 2-hydroxo or 2-amino substituent revealed that the regioselectivity is *not* determined by the electronegativity of the heteroatom and thus by the differences in the NPA charges or the resulting Coulombic interactions in the transition structures. The main reason for the observed regioselectivities is the π-donor ability of the substituent to contribute to a delocalized π system incorporating the adjacent imine moiety. The increasing π-donor capability results in decreased reactivity of this moiety and increases the (relative) reactivity of the second imine group. This effect can even overcompensate for strong intramolecular Coulombic attractions in the transition structures.

Keywords: catalysis · cycloaddition · DFT calculations · regioselectivity · transition metals

Introduction

Cycloaddition reactions represent one of the most effective and atom economic—and thus enviromentally benign—approaches to the synthesis of heterocyclic compounds. One of the major goals in the development of cycloaddition reactions is the control of the regio- and stereochemistry. Accordingly, a number of studies have been published in which the experimentally observed outcome of cycloaddition reactions that lead to heterocyclic products has been rationalized by computational methods with the aim of gaining information to allow the regio- and stereochemistry of a given reaction to be predicted. Most of the calculations were performed on dipolar cycloaddition reactions using, for example, nitrones,[1] nitrile oxides,[2] diazo compounds,[3] azides,[4] several cumulene systems,[5] aromatic nitro compounds,[6] dipolar heterocyclic systems such as sydnones[7] or muenchnones[8] or even sulfur trioxide[9] or ozone.[10] Computational studies by various groups also focused on the reactivity of nitriles or isocyanides,[11] carbenes,[12] thiocarbonyl compounds[13] or compounds with carbon–phosphorous multiple bonds[14] in cycloaddition reactions.

Recently, some of us reported the synthesis of chiral spiro-lactams from the [2+2+1] cycloaddition of a ketimine with carbon monoxide and ethylene catalyzed by ruthenium or iron carbonyl complexes (Scheme 1).[15] The starting compound is a chiral 1,4-diazabutadiene produced from enantiomerically pure L-prolinol and the corresponding bis(imidoyl)oxalyl chloride. As can be seen from Scheme 1 the cycloaddition reaction exclusively takes place at the

[a] Priv.-Doz. Dr. W. Imhof
Institute of Inorganic and Analytical Chemistry of the Friedrich-Schiller-University Jena
August-Bebel-Strasse 2, 07743 Jena (Germany)
Fax: (+49) 3641-9-48102
E-mail: Wolfgang.Imhof@uni-jena.de

[b] Prof. Dr. E. Anders
Institute of Organic Chemistry and Macromolecular Chemistry of the Friedrich-Schiller-University Jena
Humboldtstrasse 10, 07743 Jena (Germany)

 DOI: 10.1002/chem.200400215

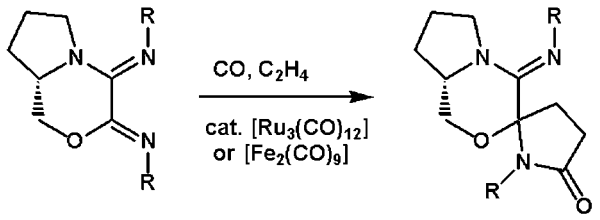

Scheme 1. Catalytic reaction of *N*,*N*-bis(aryl)tetrahydropyrrolo-[2,1*c*,1,4]oxazine-3,4-diylidenediamine with carbon monoxide and ethylene.

imine functional group adjacent to the oxazine oxygen atom. For both metal carbonyls, the regioselectivity of this reaction is 100%, whereas the overall yields in the case of $[Ru_3(CO)_{12}]$ are almost quantitative when R represents an aryl group without *ortho* substituents. Turnover numbers are somewhat lower when $[Fe_2(CO)_9]$ was used as the precatalyst.[15]

The complete catalytic cycle of this formal cycloaddition reaction has been calculated at a high level of theory.[16] A simplified catalytic cycle is depicted in Scheme 2. The cycle

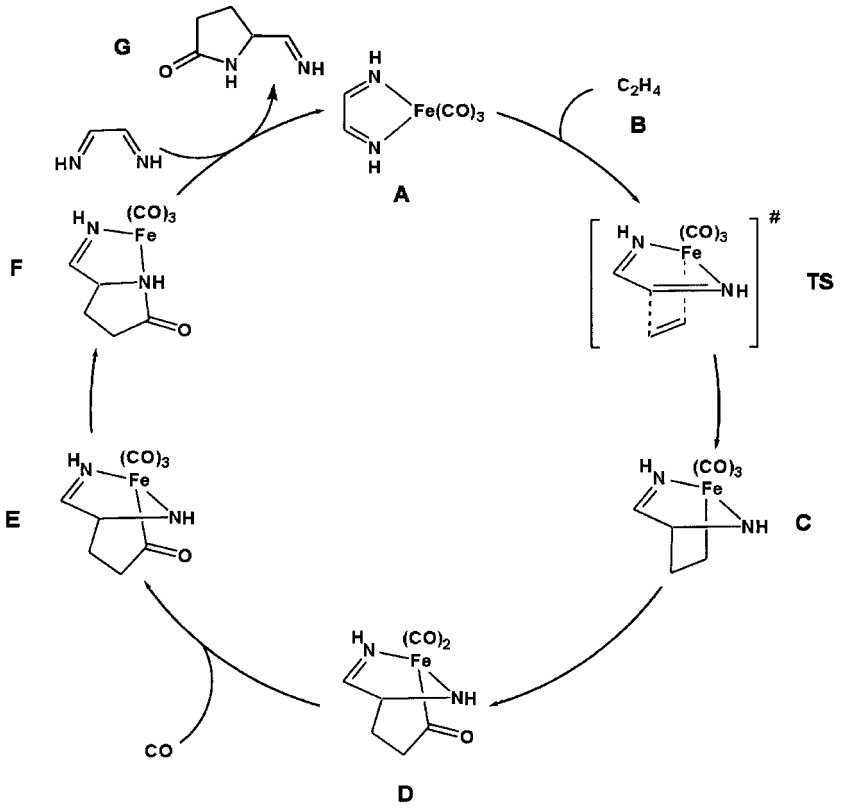

Scheme 2. Catalytic cycle of the [2+2+1] cycloaddition reaction of a diazabutadiene, carbon monoxide, and ethylene to generate lactams.

is initiated by the formation of the [(1,4-diazabutadiene)Fe-$(CO)_3$] complex **A**, in which the metal center displays a square-pyramidal coordination sphere. The catalysis is a stepwise process with the introduction of ethylene (**B**) as the *first* substrate. Ethylene adds to the starting complex **A** from the base of the square pyramid to yield the metalla-bicyclic intermediate **C** via the transition structure **TS** (Scheme 2). The formation of this transition structure also turned out to be the rate-determining step of the catalytic cycle. After insertion of a CO ligand into the C–Fe bond (formation of **D**), addition of an external molecule of carbon monoxide (to give **E**) followed by a metal-mediated ring closure via the intermediate **F**, the final product, the pyrrolidinone derivative **G** is replaced by the next 1,4-diazabutadiene substrate. This replacement step closes the catalytic cycle.

Herein we summarize the results of a theoretical study at the B3LYP/6–311++G(d,p) level of theory which provides a first systematic attempt to evaluate the influence of the "second sphere" substituents of the 1,4-diazabutadiene moiety, that is, the heteroatoms of the oxazine ring, on the regioselectivity (Scheme 1).

These calculations should provide an explanation for the experimentally observed perfect regioselectivity of the reaction and thus may be considered to be an important step towards the general prediction of the outcome of catalytic cycloaddition reactions in terms of their regio- or stereochemistry. To the best of our knowledge, to date there is no exhaustive theoretical investigation that explains the regioselective reaction of bifunctional substrates with both potential reaction sites being coordinated to the catalytically active transition metal and which include the complete catalytic cycle.

There are a few reports dealing with cycloaddition reactions in which main group or transition metals are involved. The former have essentially been investigated owing to their Lewis acid activity. The role of BF_3 or BBr_3 in the cycloaddition reaction of α,β-unsaturated aldehydes with 1,3-butadienes, which proceed via asynchronous transition structures, has been investigated by computational methods.[17] In contrast, it has been shown that the reaction of 2-azadienes with aldehydes catalyzed by BF_3 works by means of a concerted mechanism.[18] The Lewis acid coordinates to the dienophile reducing the reaction barrier and increasing the stereoselectivity by interaction with the imine lone pair. The regioselectivity of the Diels–Alder reaction of 4,5-dimethylene-2-oxazolidinones with unsymmetrical dienophiles was also highly improved by the addition of $AlCl_3$ or $TiCl_4$ as Lewis acid. Nevertheless, calculations performed on this reaction did not explain the role of the metals since they were not taken into consideration.[19]

In the cobalt-catalyzed cycloaddition of 5-hexynenitrile and 1,3-diynes leading to disubstituted 2,2′-bipyridines, the function of the transition metal has been rationalized by calculations. The regioselectivity of the reaction is ensured by the preferential coordination of the catalytically active species to an amino functional group constructed in the first uncatalyzed reaction step.[20]

The most closely related reactions with respect to the subject of our work, in which a metallacycle is formed by a formal cycloaddition reaction was described by Beckhaus et al. The reaction of a titanocene vinylidene complex with alkynes, diynes, or isothiocyanates results in methylene-metallacyclobutenes or methylene-metallathietane complexes, respectively.[21] The regioselectivities of the cycloaddition reactions may be attributed to the polarity of the substituted alkyne substrates or the lower polarity of the C=S bond compared to the C=N bond in the latter case.

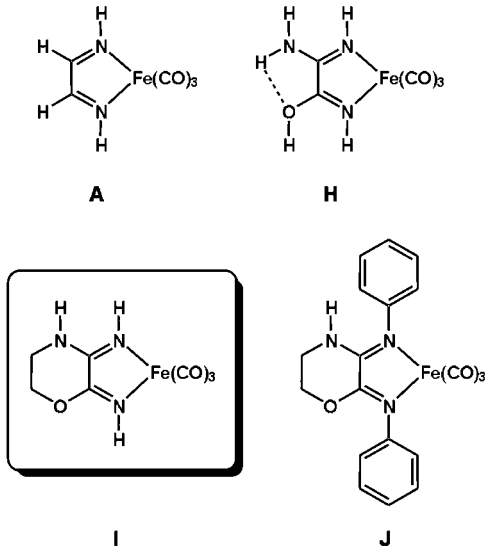

Scheme 3. Different degrees of simplification leading to the model used in the calculations.

Computational Methods

Full-geometry optimizations (i.e. without symmetry constraints) were carried out with the GAUSSIAN98 program package[22] in which the hybrid Hartree–Fock DFT approach (B3LYP/6–311++G(d,p)) was used throughout.[23] The density functional employed contains a term which accounts for the effects of dynamic electron correlation (Coulomb hole).[24] Use of a basis set with triple ζ quality[25] and which contains diffuse functions allows a better consideration of weakly bound (i.e. van der Waals) complexes, H-bridged species, and a variety of interacting electron lone pairs. The B3LYP functional has previously been found to be of a suitable theoretical level for the study of the interactions of transition metals with ligands, especially with CO.[26]

Suitable starting geometries concerning the coordination sphere of the iron atom were taken from the calculation of the complete catalytic cycle of this cycloaddition reaction.[16] Stationary points were rigorously characterized as minima or transition states according to the number of imaginary modes by applying a second-order derivative calculation (vibrational analysis).[27] Visualization of the reactive mode in the transition structures was used to support the assignments of the pertaining minimum structures. Zero-point energy (ZPE) corrections have been made.

Thermochemistry calculations were performed by using the standard routine in GAUSSIAN98, Version A11 (for details see Gaussian 98 User's Reference, Gaussian Inc., Carnegie Office Park, Building 6, Pittsburg, PA, USA) or the freqchk routine in conjunction with the final checkpoint file resulting from successful frequency calculations.[28] Reed and Weinhold's natural bond orbital (NBO) analysis[29] was used to calculate natural atomic charges.

Results and Discussion

First of all we had to decide on the model compound for the calculations. Scheme 3 shows four different degrees of simplification. The pyrrolidine system—present in the system used experimentally because prolinol was used as the starting compound (Scheme 1)—was omitted in all cases. Compound type **A** (Scheme 2, 3) was used to calculate the complete catalytic cycle of this cycloaddition reaction, but due to its symmetry **A** is not suitable for discriminating between the two imine moieties. Compound type **H** has an amino and a hydroxy substituent in the "second sphere" along the diazadiene backbone, which allows a differentiation between the two C=N bonds. It is however obvious that we have to expect strong intramolecular hydrogen bonding effects, which will influence the bonding in the 1,4-diazabutadiene substrate both electronically and sterically. Compound type **J** is very close to the system used in the experiments, but the basis sets for calculations at a high level of theory would be extremely large. Compound type **I** seems to be the best compromise for a suitable model substrate in which the bonding closely resembles that in the real substrate, and the basis set is of a workable size.

Scheme 4 shows the two elementary steps of the catalytic cycloaddition reaction that we investigated in the course of this work. The addition of ethylene (**B**) to the cyclic (1,4-diazabutadiene)$Fe(CO)_3$ complex $\mathbf{I_1}$ from the base of the square-pyramidal coordination sphere of iron was shown to be the rate-determining step of the whole reaction sequence.[16] In addition, these elementary steps produce the new C–C bond between ethylene and the competing imine-carbon atoms, and thus determine the regioselectivity of the complete cycloaddition (Scheme 1). This reaction can also be interpreted as a [3+2] cycloaddition reaction in which a metal is involved leading to a new ferra-pyrrolidine ring and thus is closely related to the formation of titanacyclobutenes.[21] The addition of ethylene leads to the diastereomeric transition states $\mathbf{TS_1}$ and $\mathbf{TS_2}$, in which a new C–C bond is formed between ethylene and the imine functional group next to the oxazine nitrogen atom. Alternatively, the new C–C bond is established between ethylene and the imine functional group next to the oxazine oxygen atom ($\mathbf{TS_3}$, $\mathbf{TS_4}$); these products reflect the experimentally observed regioselectivity. The transition states $\mathbf{TS_1}$–$\mathbf{TS_4}$ then produce the intermediates $\mathbf{P_1}$–$\mathbf{P_5}$. There is more than one transition structure and more than one product for each reaction channel because different conformations of the oxazine ring system have to be taken into account. The methylene groups of the oxazine may be situated above or below the plane formed by the imine functional groups and the heteroatoms of the oxazine. Another way to describe the

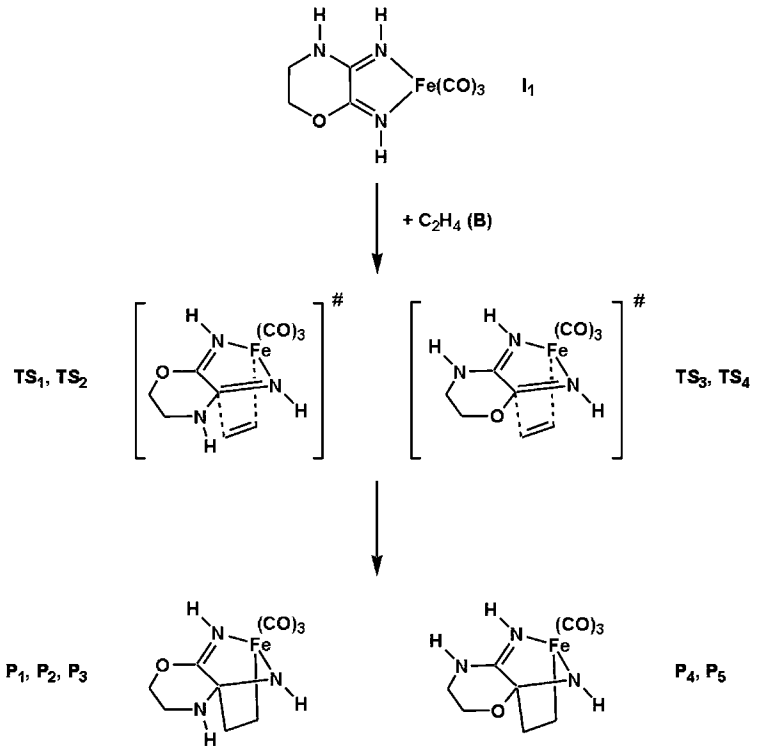

Scheme 4. The addition of ethylene to $\mathbf{I_1}$ leading to $\mathbf{TS_1}$–$\mathbf{TS_4}$ and $\mathbf{P_1}$–$\mathbf{P_5}$.

different conformations would be that the apical carbon monoxide ligand may be situated on both sides of the above-mentioned substrate plane leading to the same conformers.

Figures 1–3 show the calculated structures for the starting compound $\mathbf{I_1}$, the transition states $\mathbf{TS_1}$–$\mathbf{TS_4}$, and the intermediates $\mathbf{P_1}$–$\mathbf{P_5}$. Specific bond lengths are summarized in Table 1. The calculated molecular structure of $\mathbf{I_1}$ is presented in Figure 1. The bond lengths of $\mathbf{I_1}$ are typical for a (1,4-diazabutadiene)$Fe(CO)_3$ complex. The C=N bonds are slightly elongated due to back donation from d orbitals of the iron atom into π^* orbitals of the imine double bonds. In addition, the C4–N3 and C5–O4 bonds are shorter than normal single bonds because of a delocalization of electron density between the imine double bonds and the heteroatoms of the oxazine system. The imine functional group next to the oxazine oxygen atom (C5=N2) seems to be a more efficient donor site for the coordination of the $Fe(CO)_3$ group, because the Fe–N2 bond is 2.0 pm shorter than the corresponding Fe–N1 bond (Table 1). The coordination sphere of iron is a square pyramid in which the iron atom is situated slightly above the base of the pyramid

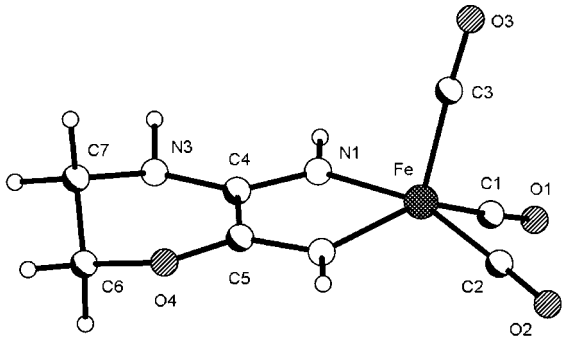

Figure 1. Structure of $\mathbf{I_1}$ optimized at the B3LYP/6–311++G(d,p) level. Bond lengths are given in Table 1.

Table 1. Calculated bond lengths [pm] of $\mathbf{I_1}$, $\mathbf{TS_1}$–$\mathbf{TS_4}$ and $\mathbf{P_1}$–$\mathbf{P_5}$; Calculations performed at the B3LYP/6–311++G(d,p) level.

	$\mathbf{I_1}$	$\mathbf{TS_1}$	$\mathbf{TS_2}$	$\mathbf{TS_3}$	$\mathbf{TS_4}$	$\mathbf{P_1}$	$\mathbf{P_2}$	$\mathbf{P_3}$	$\mathbf{P_4}$	$\mathbf{P_5}$
Fe–C1	179.7	180.2	180.1	179.8	179.1	181.2	181.3	181.2	178.4	180.9
C1–O1	115.0	114.5	114.6	114.6	114.6	114.3	114.3	114.3	114.4	114.4
Fe–C2	179.5	179.0	180.3	180.6	180.0	178.4	178.3	178.3	180.9	178.4
C2–O2	114.8	114.6	114.6	114.6	114.6	114.4	114.4	114.4	114.4	114.4
Fe–C3	179.2	180.5	179.3	179.0	179.8	184.9	184.7	184.8	184.6	184.9
C3–O3	114.9	114.2	114.2	114.4	114.4	113.8	113.9	113.9	113.9	113.8
Fe–N1	196.7	196.4	196.8	200.0	199.9	202.6	202.1	203.1	203.6	203.5
Fe–N2	194.7	199.9	198.8	195.7	195.4	203.4	203.6	202.9	203.3	202.2
N1–C4	131.8	135.7	135.4	130.1	130.4	144.7	145.2	145.8	129.3	129.2
N2–C5	131.1	129.3	129.5	134.3	134.6	127.9	127.9	128.0	143.9	143.3
C4–C5	142.2	145.5	145.0	146.2	145.9	152.3	152.6	152.1	152.8	152.7
C4–N3	139.1	142.0	142.8	137.0	136.6	146.9	146.5	147.1	135.0	135.2
C5–O4	136.3	134.8	135.0	138.8	138.9	133.5	133.4	133.1	143.5	143.8
O4–C6	144.0	144.9	144.9	142.9	143.0	145.9	145.9	146.0	141.8	141.7
C6–C7	152.3	151.8	152.5	152.4	152.2	152.2	152.2	151.4	152.3	152.2
N3–C7	146.4	146.1	146.3	146.5	146.1	146.1	145.6	145.8	147.0	146.8
C8–C4	–	210.3	211.7	–	–	156.0	156.0	156.1	–	–
C8–C5	–	–	–	210.2	209.7	–	–	–	155.0	155.7
C8–C9	–	142.3	141.5	141.1	140.8	153.0	152.7	152.7	152.7	152.8
Fe–C9	–	247.8	253.3	258.4	259.5	211.7	211.3	211.6	211.5	211.5

(N1, N2, C1, and C2). The geometry of the bonds around N3 lies somewhere between a planar and a tetrahedral arrangement with the sum of bond angles of 345.6°. This transition from tetrahedral coordination (sum of bond angles 328.5° without consideration of the lone pair) towards planarity (sum of bond angles 360°) is also attributed to the delocalization of electron density between N1, C4, and N3.

The transition states $\mathbf{TS_1}$–$\mathbf{TS_4}$ are depicted in Figure 2, and specific bond lengths are given in Table 1. All the transition states are formed by the addition of ethylene to $\mathbf{I_1}$ from the base of the square-pyramidal coordination sphere around iron. $\mathbf{TS_1}$ and $\mathbf{TS_2}$ arise from an addition of the ethylene carbon atom C8 to the carbon atom next to the oxazine nitrogen atom (C4), whereas in $\mathbf{TS_3}$ and $\mathbf{TS_4}$ a new C–C bond (C5–C8) to the imine group next to the oxazine oxygen atom is produced. In general, the bond lengths in $\mathbf{TS_1}$–$\mathbf{TS_4}$ show some similar trends to those in the corresponding substrate $\mathbf{I_1}$. The interaction between C9 and Fe produces an octahedral coordination geometry around the iron center. Nevertheless, this interaction in all cases is quite weak and the bond lengths fall in the range 248–260 pm. The interaction between C8 and C4 ($\mathbf{TS_1}$, $\mathbf{TS_2}$) or C5 ($\mathbf{TS_3}$, $\mathbf{TS_4}$) shows bond lengths of 210–212 pm. The bond between C8 and C9 is elongated compared to the C–C bond in free ethylene (134.8 pm[16]) by about 6 pm.

The former imine nitrogen atom next to the carbon atom that interacts with ethylene formally becomes a more negatively charged amide donor compared with the imine nitrogen atoms in $\mathbf{I_1}$. The N–Fe bond lengths of this nitrogen atom (N1 in $\mathbf{TS_1}$ and $\mathbf{TS_2}$, N2 in $\mathbf{TS_3}$ and $\mathbf{TS_4}$) to iron are shorter than the distances between the unaffected imine nitrogen atoms, such as N2 in $\mathbf{TS_1}$, and the metal center. In $\mathbf{TS_1}$ and $\mathbf{TS_2}$ this difference is 3.5 and 2.0 pm, respectively, whereas the corresponding bond lengths in $\mathbf{TS_3}$ and $\mathbf{TS_4}$ differ by 4.3 and 4.5 pm, respectively.

Another interesting difference in the bonding modes in the transition structures that are produced by the addition of ethylene to the imine subunit next to the oxazine nitrogen atom ($\mathbf{TS_1}$, $\mathbf{TS_2}$) compared to $\mathbf{TS_3}$ and $\mathbf{TS_4}$ is related to the geometry around N3. In $\mathbf{TS_1}$ and $\mathbf{TS_2}$ the sum of angles around N3 is 339.1 and 335.9°, respectively. Compared to the situation in $\mathbf{I_1}$ this indicates a shift towards a more tetrahedral coordination mode for N3. In contrast $\mathbf{TS_3}$ and $\mathbf{TS_4}$ show a nearly perfectly planar arrangement around N3 with a sum of angles of 353.3 and 357.2°, respectively. Obviously, in $\mathbf{TS_1}$ and $\mathbf{TS_2}$ N3 is no longer part of a delocalized system, whereas the delocalization is at its optimum for $\mathbf{TS_3}$ and $\mathbf{TS_4}$.

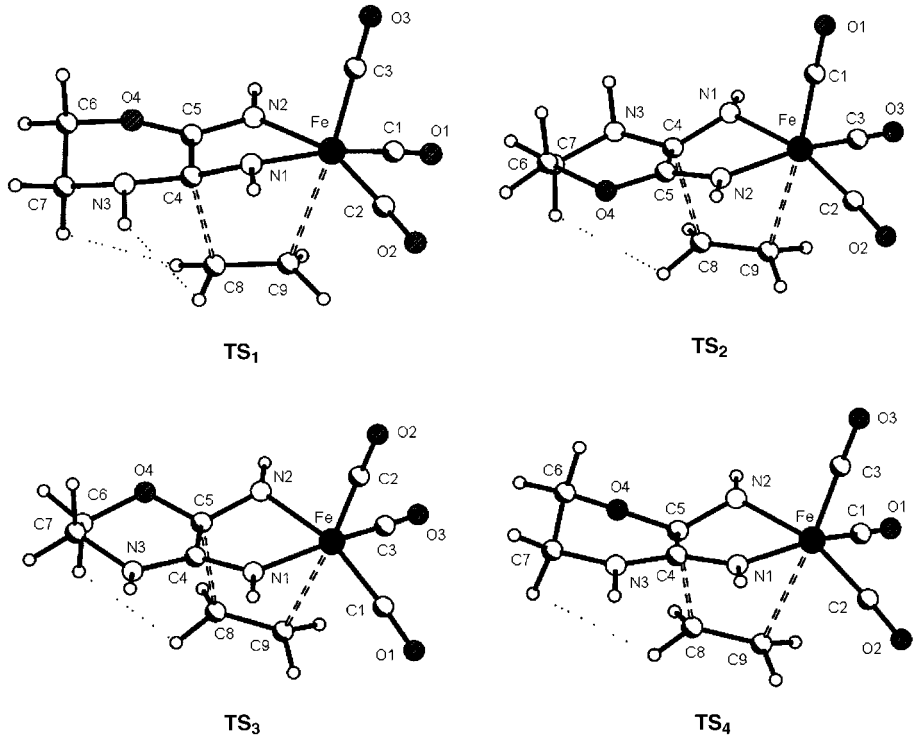

Figure 2. Structures of $\mathbf{TS_1}$–$\mathbf{TS_4}$ optimized at the B3LYP/6–311++G(d,p) level. Bond lengths are given in Table 1.

The conformations of the oxazine ring that resulted from our calculations basically differ by 1,2-, 1,3-, or 1,4-interactions of the hydrogen atoms of ethylene with protons at the oxazine ring. In $\mathbf{TS_1}$ there is one interaction with the axial hydrogen atom at C7 (249.2 pm) and another one with the proton at N3 (255.9 pm). In $\mathbf{TS_2}$ the interaction between ethylene and the axial proton at C7 is still there although it is much weaker (252.5 pm). The proton at N3 adopts a position *trans* to ethylene in this case. $\mathbf{TS_3}$ also shows a quite short interaction between ethylene and the axial hydrogen atom at C6 (242.9 pm), whereas the shortest contact in $\mathbf{TS_4}$ is observed between ethylene and a hydrogen atom at C7, which is much weaker (286.1 pm).

The calculated molecular structures of $\mathbf{P_1}$–$\mathbf{P_5}$ are depicted in Figure 3, and specific bond lengths are listed in Table 1. Following the reaction coordinate from the transition states to the intermediates $\mathbf{P_1}$–$\mathbf{P_5}$, again leads to some similar trends for all products compared to the situation in $\mathbf{TS_1}$–$\mathbf{TS_4}$. The coordination sphere around the iron center is octahedral. The Fe–C9 bond length is very similar in all products (211.3–211.7 pm). The carbon monoxide ligand *trans* to the formally carbanionic center at C9 shows the longest Fe–C_{CO} bond and, correspondingly, the shortest C–O bond length. The Fe–N bonds are longer than in the transition states. The differences between the Fe–N bonds in the same molecule are between 0.2–1.5 pm in $\mathbf{P_1}$–$\mathbf{P_5}$.

Each molecule exhibits one C–N bond that is clearly a double bond (N2–C5 in $\mathbf{P_1}$–$\mathbf{P_3}$, N1–C4 in $\mathbf{P_4}$ and $\mathbf{P_5}$) with a

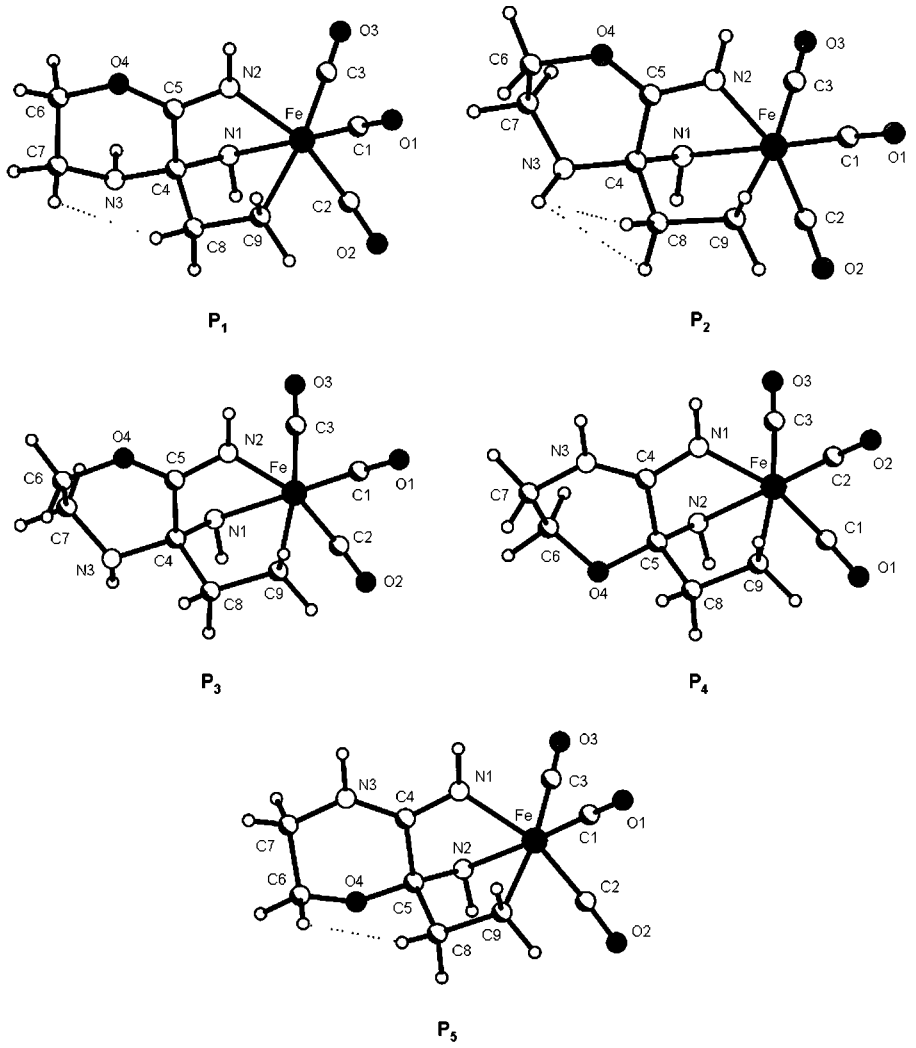

Figure 3. Structures of $\mathbf{P_1}$–$\mathbf{P_5}$ optimized at the B3LYP/6–311++G(d,p) level. Bond lengths are given in Table 1.

bond length of 127.9 pm in $\mathbf{P_1}$–$\mathbf{P_3}$ and 129.3 pm in $\mathbf{P_4}$ and $\mathbf{P_5}$. This difference is clearly due to the fact that the imine group is situated next to the oxazine nitrogen atom in $\mathbf{P_1}$–$\mathbf{P_3}$ and next to the oxazine oxygen atom in $\mathbf{P_4}$ and $\mathbf{P_5}$. All the remaining bond lengths are consistent with single bonds between the corresponding atoms.

The bonding around N3 shows the same trend as for the transition states $\mathbf{TS_1}$–$\mathbf{TS_4}$. All products in which a new C–C bond is established between C8 and the imine group next to the oxazine nitrogen atom show a nearly perfect tetrahedral coordination of N3 (sum of bond angles $\mathbf{P_1}$: 330.9°, $\mathbf{P_2}$: 334.5°, $\mathbf{P_3}$: 333.5°). On the other hand, all compounds that were produced by the addition of ethylene to the imine group next to the oxazine oxygen atom show a perfectly planar arrangement of substituents around N3 (sum of angles $\mathbf{P_4}$: 357.7°, $\mathbf{P_5}$: 355.9°). This observation is attributed to the fact that the possibility of establishing the delocalization of any electron density from N3 to a π system is only present in $\mathbf{P_4}$ and $\mathbf{P_5}$.

The conformers depicted in Figure 3 again differ mostly by variations of 1,2- and 1,3-interactions of hydrogen atoms at C8 with some protons of the oxazine ring system. $\mathbf{P_3}$ and $\mathbf{P_4}$ show no short contacts of this type. In $\mathbf{P_1}$ quite a short interaction between protons at C8 and C7 (235.4 pm) is observed. A similar interaction may be seen in $\mathbf{P_5}$ between hydrogen atoms at C8 and C6 (223.8 pm). In $\mathbf{P_2}$ both hydrogen atoms at C8 are in close contact to the proton at N3 (240.0 pm, 245.1 pm).

Table 2 summarizes the calculated total energies of the reactants $\mathbf{I_1}$ and **B**, the transition states $\mathbf{TS_1}$–$\mathbf{TS_4}$, and the product complexes $\mathbf{P_1}$–$\mathbf{P_5}$. In addition, thermal and entropic corrections have been applied, since the experimental cycloaddition reactions were carried out at a reaction temperature of 438 K and a pressure of 20 atm.[15a,16] We have also shown that the reaction works quantitatively with lower pressures down to 1.5 atm.[15b] The reaction conditions of 438 K and 10 atm are therefore realistic. Figure 4 shows the energy profiles of the addition of ethylene, **B**, to [(1,4-diazabutadiene)$Fe(CO)_3$], $\mathbf{I_1}$. In Table 3 the relative Gibbs free energies of elementary steps leading to the stationary points of the reactions are given.

Table 2. Calculated total energies E, energies after thermal and entropic corrections at 298.15 K and 1 atm (E_{c1}), and energies after thermal and entropic corrections at 438 K and 10 atm (E_{c2}) for **B**, $\mathbf{I_1}$, $\mathbf{TS_1}$–$\mathbf{TS_4}$ and $\mathbf{P_1}$–$\mathbf{P_5}$.[a]

Compound	$-E$ [a.u.]	[Nimag][b]	ZPE [kcal mol^{-1}]	$-E_{c1}$ [a.u.]	$-E_{c2}$ [a.u.]
B	78.6155382	[0]	31.87	78.5862822	78.5965222
$\mathbf{I_1}$	2000.0934433	[0]	93.65	1999.9879433	2000.0154383
$\mathbf{TS_1}$	2078.6675927	[1]	126.87	2078.5095777	2078.5388527
$\mathbf{TS_2}$	2078.666917	[1]	127.01	2078.508616	2078.537814
$\mathbf{TS_3}$	2078.6711452	[1]	126.74	2078.5134482	2078.5428592
$\mathbf{TS_4}$	2078.6704107	[1]	126.49	2078.5136397	2078.5433877
$\mathbf{P_1}$	2078.6981395	[0]	129.30	2078.5355555	2078.5641055
$\mathbf{P_2}$	2078.6957439	[0]	129.18	2078.5335849	2078.5622929
$\mathbf{P_3}$	2078.696566	[0]	129.14	2078.534616	2078.563413
$\mathbf{P_4}$	2078.7066372	[0]	129.13	2078.5445532	2078.5733082
$\mathbf{P_5}$	2078.7042162	[0]	129.12	2078.5419262	2078.5705382

[a] All calculations performed at the B3LYP/6–311++G(d,p) level. [b] Number of imaginary frequencies.

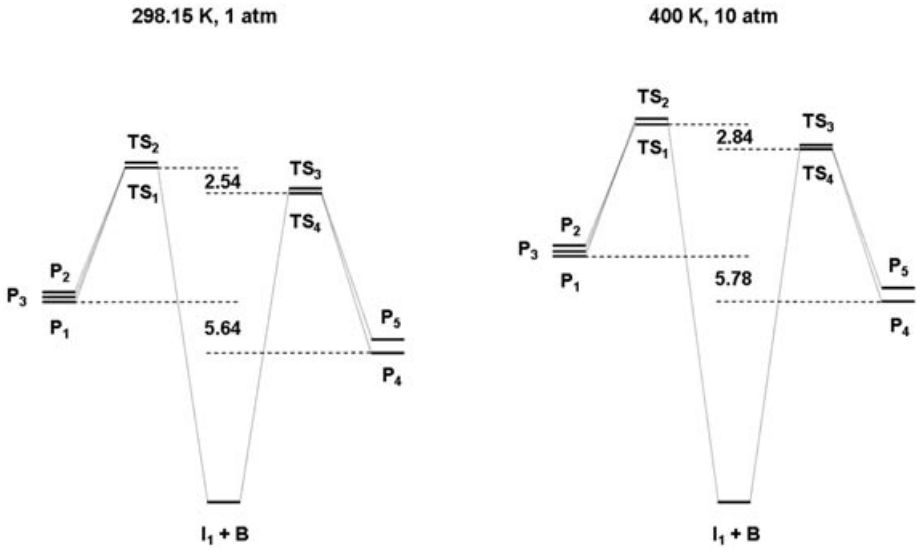

Figure 4. The interaction of ethylene with $\mathbf{I_1}$ at different temperatures and pressures. For relative free energies of $\mathbf{I_1}$, $\mathbf{TS_1}$–$\mathbf{TS_4}$, and $\mathbf{P_1}$–$\mathbf{P_5}$ see Table 2.

Table 3. Relative Gibbs free energies of elementary steps leading to $\mathbf{TS_1}$–$\mathbf{TS_4}$ and $\mathbf{P_1}$–$\mathbf{P_5}$.

Elementary step (298.15 K, 1 atm)	ΔG [kcal mol^{-1}][a]	Elementary step (438 K, 10 atm)	ΔG [kcal mol^{-1}][a]
$\mathbf{B + I_1 \rightarrow TS_1}$	40.56	$\mathbf{B + I_1 \rightarrow TS_1}$	45.87
$\mathbf{B + I_1 \rightarrow TS_2}$	41.17	$\mathbf{B + I_1 \rightarrow TS_2}$	46.53
$\mathbf{B + I_1 \rightarrow TS_3}$	38.14	$\mathbf{B + I_1 \rightarrow TS_3}$	43.35
$\mathbf{B + I_1 \rightarrow TS_4}$	38.02	$\mathbf{B + I_1 \rightarrow TS_4}$	43.03
$\mathbf{TS_1 \rightarrow P_1}$	−16.30	$\mathbf{TS_1 \rightarrow P_1}$	−15.84
$\mathbf{TS_1 \rightarrow P_2}$	−15.06	$\mathbf{TS_1 \rightarrow P_2}$	−14.71
$\mathbf{TS_1 \rightarrow P_3}$	−15.71	$\mathbf{TS_1 \rightarrow P_3}$	−15.41
$\mathbf{TS_4 \rightarrow P_4}$	−19.40	$\mathbf{TS_4 \rightarrow P_4}$	−18.78
$\mathbf{TS_4 \rightarrow P_5}$	−17.75	$\mathbf{TS_4 \rightarrow P_5}$	−17.04

[a] Values have been determined taking frequency calculations into consideration.

Activation barriers: In comparison with the symmetrical model complex **A** (Scheme 2,3), the "second sphere" atoms N and O of the oxazine ring both cause the decrease of the activation barriers for the ethylene addition, which for the addition of **A** to **B** via $\mathbf{TS_{A-B}}$ is 42.6 kcal mol^{-1} (298.15 K, 1 atm).[16] In the case of the most stable transition states, $\mathbf{TS_1}$ and $\mathbf{TS_4}$, the oxazine nitrogen atom lowers this barrier ($\mathbf{TS_1}$) by just 2.0 kcal mol^{-1}, whereas the corresponding value for the alternative addition via $\mathbf{TS_4}$ at the oxazine oxygen atom site is significantly lower (4.6 kcal mol^{-1}). In other words, $\mathbf{TS_4}$ is the transition state that is lowest in energy; it is, 2.5 kcal mol^{-1} (298.15 K, 1 atm) or 2.8 kcal mol^{-1} (438 K, 10 atm) more stable than the lowest transition state for an addition of ethylene to the carbon atom next to the oxazine nitrogen atom ($\mathbf{TS_1}$).

It is obvious that there are no significant differences in the selectivity of the reaction under the different reaction conditions (Table 3, Figure 4).

The conformeric transition states and products $\mathbf{TS_1}$ and $\mathbf{TS_2}$, $\mathbf{TS_3}$ and $\mathbf{TS_4}$, $\mathbf{P_1}$–$\mathbf{P_3}$ as well as $\mathbf{P_4}$ and $\mathbf{P_5}$ are so close in energy that they interconvert at the temperatures chosen for the calculations. In addition, the stabilization connected with the formation of $\mathbf{P_1}$ from $\mathbf{TS_1}$ is considerably lower than the corresponding energy in the reaction of $\mathbf{TS_4}$ to $\mathbf{P_4}$ (−16.30 kcal mol^{-1} versus −19.40 kcal mol^{-1} at 298.15 K, 1 atm and −15.84 kcal mol^{-1} versus −18.78 kcal mol^{-1} at 438 K, 10 atm, Table 3). The formation of adducts of ethylene with **I** forming product complexes in which the new C–C bond is established next to the oxazine oxygen atom is favored thermodynamically due to the relative product stability as well as kinetically because of the higher activation barrier of a potential reverse reaction (cf. the relative energies of $\mathbf{TS_1}$, $\mathbf{TS_2}$, Figure 4).

NPA charges: Table 4 shows the NPA charges of selected atoms of $\mathbf{I_1}$ and the transition states $\mathbf{TS_1}$–$\mathbf{TS_4}$. It can be seen that Fe exhibits almost identical values for all transition states. The charges of the imine-nitrogen atoms (N1, N2) are shifted to more negative values on the addition of ethylene. The carbon atoms of ethylene also show very similar charges. The most significant differences are observed for the values calculated for C4 and C5. If the new C–C bond is established to the imine group next to the oxazine nitrogen atom ($\mathbf{TS_1}$, $\mathbf{TS_2}$) the NPA charge at C4 is lower than that in the substrate **I**, whereas the corresponding charge at C5 is enhanced. For $\mathbf{TS_3}$ and $\mathbf{TS_4}$, where ethylene is added to the carbon atom next to the oxazine oxygen atom, higher charges are observed at C4 and C5. In summary, this leads to a much higher difference in the NPA charges between the carbon atom C8 of ethylene and the imine-carbon atom of **I** to which it is added for $\mathbf{TS_3}$ and $\mathbf{TS_4}$. Since this regioselectivity is the one that is exclusively observed in the experiments, it appears to be conceivable that Coulombic interactions determine the regioselectivity of this cycloaddition to a significant extent.

Table 4. NPA charges of selected atoms of $\mathbf{I_1}$ and $\mathbf{TS_1}$–$\mathbf{TS_4}$. Calculations performed at the B3LYP/6–311++G(d,p) level.

	$\mathbf{I_1}$	$\mathbf{TS_1}$	$\mathbf{TS_2}$	$\mathbf{TS_3}$	$\mathbf{TS_4}$
Fe	−0.03	−0.10	−0.09	−0.09	−0.09
N1	−0.69	−0.81	−0.81	−0.71	−0.72
N2	−0.68	−0.71	−0.71	−0.80	−0.80
C4	0.32	0.29	0.29	0.42	0.41
C5	0.45	0.58	0.56	0.45	0.45
N3	−0.64	−0.66	−0.67	−0.63	−0.63
O4	−0.55	−0.55	−0.55	−0.58	−0.58
C8	–	−0.46	−0.44	−0.47	−0.45
C9	–	−0.50	−0.49	−0.47	−0.47

The differences in the NPA charges suggest that the electronegativity—or σ-acceptor ability—of the substituents in 1,4-diazabutadienes determine the regioselectivities. On the other hand, as we pointed out before, one interesting property of the transition structures and products concerns the coordination geometry around the oxazine nitrogen atom. This property of course corresponds to the ability of this amino group to act as a π donor establishing a delocalized π-electron system incorporating the adjacent imine group. To determine whether the σ-donor or the π-acceptor capacities are the decisive factor for the observed regioselectivities we calculated the analogous reaction of ethylene with a 1,4-diazabutadiene bearing either a fluoro, hydroxo, or amino substituent in the 2-position. If the σ-acceptor ability were to prove the most important influence, the regioselectivity would be at its optimium in the case of the fluoro substituent. If the π-donor ability was in fact the crucial influence determining regioselectivity, the amino function would represent the most selective derivative.

Scheme 5 shows the iron tricarbonyl complexes $\mathbf{I_2}$–$\mathbf{I_4}$ of the three 2-substituted 1,4-diazabutadiene ligands. The calculated transition structures and products together with the corresponding bond lengths are summarized in Figure 5 and Table 5 (F-substituted), Figure 6 and Table 6 (OH-substituted), Figure 7 and Table 7 (NH_2-substituted).

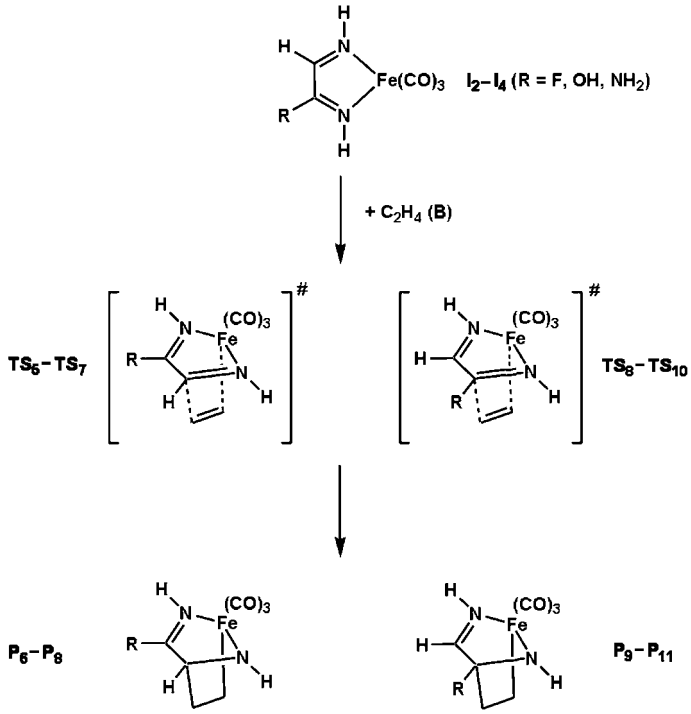

Scheme 5. The addition of ethylene to $\mathbf{I_2}$–$\mathbf{I_4}$ leading to $\mathbf{TS_5}$–$\mathbf{TS_{10}}$ and $\mathbf{P_6}$–$\mathbf{P_{11}}$.

The bond lengths for $\mathbf{I_2}$–$\mathbf{I_4}$, $\mathbf{TS_5}$–$\mathbf{TS_{10}}$, and $\mathbf{P_6}$–$\mathbf{P_{11}}$ show similar trends to those described for the transition structures and products mentioned above. The approach of ethylene during the formation of $\mathbf{TS_5}$–$\mathbf{TS_{10}}$ leads to an elongation of the C–C bond in ethylene itself. In addition, the C–N bond of the imine group that does not interact with ethylene is shorter than that in the corresponding starting compound $\mathbf{I_2}$–$\mathbf{I_4}$, whereas the other imine bond is also elongated. Inter-

Table 5. Calculated bond lengths [pm] of $\mathbf{I_2}$, $\mathbf{TS_5}$, $\mathbf{TS_8}$, $\mathbf{P_6}$, and $\mathbf{P_9}$ (R = F). Calculations performed at the B3LYP/6–311++G(d,p) level.

	$\mathbf{I_2}$	$\mathbf{TS_5}$	$\mathbf{TS_8}$	$\mathbf{P_6}$	$\mathbf{P_9}$
Fe–C1	180.3	180.9	180.4	181.6	181.3
C1–O1	114.5	114.3	114.4	114.3	114.2
Fe–C2	181.1	179.1	179.9	178.0	178.9
C2–O2	114.5	114.4	114.4	114.4	114.2
Fe–C3	179.2	180.2	180.2	185.1	185.2
C3–O3	114.5	114.1	114.1	113.7	113.7
Fe–N1	195.3	200.3	196.9	206.2	202.8
Fe–N2	190.5	195.1	197.0	201.9	202.4
N2–C4	133.8	136.0	129.8	145.8	127.2
N1–C5	131.0	128.5	134.0	126.5	142.3
C4–C5	139.4	142.8	143.5	149.3	150.6
C5–F	134.6	134.3	137.1	133.7	141.6
C4–C6	–	208.6	–	156.1	–
C5–C6	–	–	206.3	–	154.8
C6–C7	–	141.9	141.3	153.3	153.0
Fe–C7	–	253.5	256.4	212.2	213.2

Table 6. Calculated bond lengths [pm] of $\mathbf{I_3}$, $\mathbf{TS_6}$, $\mathbf{TS_9}$, $\mathbf{P_7}$, and $\mathbf{P_{10}}$ (R = OH). Calculations performed at the B3LYP/6–311++G(d,p) level.

	$\mathbf{I_3}$	$\mathbf{TS_6}$	$\mathbf{TS_9}$	$\mathbf{P_7}$	$\mathbf{P_{10}}$
Fe–C1	179.9	180.6	180.5	181.3	181.3
C1–O1	114.6	114.4	114.4	114.4	114.3
Fe–C2	180.7	179.2	179.7	178.0	178.8
C2–O2	114.6	114.5	114.4	114.4	114.3
Fe–C3	179.5	179.8	180.5	184.8	184.8
C3–O3	114.6	114.2	114.1	113.8	113.8
Fe–N1	195.9	199.5	196.5	205.4	202.2
Fe–N2	189.7	194.4	197.5	201.7	202.1
N2–C4	133.7	135.8	129.6	145.7	127.3
N1–C5	131.4	129.3	134.9	128.1	144.5
C4–C5	140.6	144.2	144.6	150.1	151.2
C5–O4	136.0	135.4	138.9	134.0	142.2
C4–C6	–	209.3	–	155.8	–
C5–C6	–	–	205.8	–	155.2
C6–C7	–	141.3	142.7	153.3	153.0
Fe–C7	–	259.3	246.4	212.1	213.2

Table 7. Calculated bond lengths [pm] of $\mathbf{I_4}$, $\mathbf{TS_7}$, $\mathbf{TS_{10}}$, $\mathbf{P_8}$, and $\mathbf{P_{11}}$ (R = NH_2). Calculations performed at the B3LYP/6–311++G(d,p) level.

	$\mathbf{I_4}$	$\mathbf{TS_7}$	$\mathbf{TS_{10}}$	$\mathbf{P_8}$	$\mathbf{P_{11}}$
Fe–C1	179.6	180.3	180.5	181.0	181.4
C1–O1	114.7	114.6	114.4	114.4	114.3
Fe–C2	180.2	179.1	179.4	178.1	178.5
C2–O2	114.8	114.6	114.4	114.5	114.3
Fe–C3	179.7	179.6	180.0	184.6	184.5
C3–O3	114.7	114.3	114.0	113.9	113.8
Fe–N1	196.7	199.6	197.1	204.1	201.4
Fe–N2	189.9	194.0	197.6	202.0	202.2
N2–C4	133.2	135.5	129.8	145.4	127.4
N1–C5	132.2	130.5	136.4	129.2	136.4
C4–C5	141.4	144.9	144.3	151.0	144.3
C5–N3	138.9	137.5	142.2	135.6	145.8
C4–C6	–	209.4	–	155.6	–
C5–C6	–	–	205.4	–	156.3
C6–C7	–	141.1	143.7	153.3	152.9
Fe–C7	–	261.5	239.7	212.0	212.6

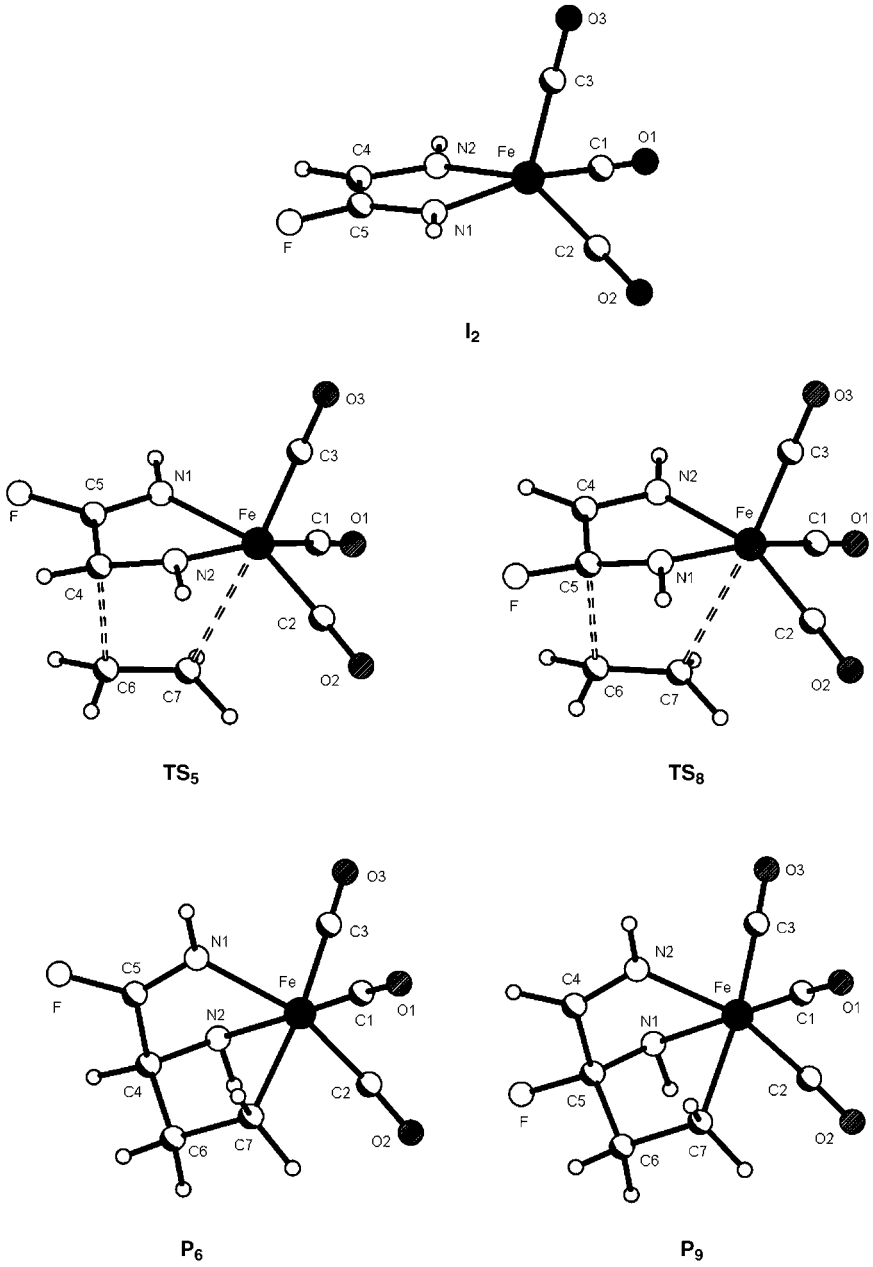

Figure 5. Structures of $\mathbf{I_2}$, $\mathbf{TS_5}$, $\mathbf{TS_8}$, $\mathbf{P_6}$, and $\mathbf{P_9}$ optimized at the B3LYP/6–311++G(d,p) level. Bond lengths are given in Table 5.

estingly, the bond length of the imine bond next to the heteroatom increases in the order $F < OH < NH_2$ no matter whether ethylene adds to this double bond or not. The remaining C–N double bond is almost unaffected by the heteroatom. The central C–C bond of the 1,4-diazabutadiene is also longer for all transition structures $\mathbf{TS_5}$–$\mathbf{TS_{10}}$ than for $\mathbf{I_2}$–$\mathbf{I_4}$ due to the loss of delocalization in the parent 1,4-diazabutadiene system.

The formation of the products $\mathbf{P_6}$–$\mathbf{P_{11}}$ from $\mathbf{TS_5}$–$\mathbf{TS_{10}}$ also leads to changes in the respective bond lengths, as expected. Nevertheless, it should be noted that there are differences if ethylene is added to the imine bond bearing the heteroatom substituent (N1–C5) or to the imine function with a hydrogen atom as the substituent at the imine-carbon atom (N2–C4). In the latter case the new Fe–C bond is always shorter than that in the isomers in which ethylene is bound to C5. In addition, the C6–C4 bonds are always slightly longer than the C6–C5 bonds in the isomeric compounds.

The C–N bond lengths depend on the nature of the heteroatom: For R = F the C–N double bond in $\mathbf{P_6}$ (C5–N1) is shorter than the corresponding bond in $\mathbf{P_9}$ (C4–N2). On the other hand, the C–N single bond in $\mathbf{P_6}$ (C4–N2) is longer than the C5–N1 bond in $\mathbf{P_9}$. For R = OH or NH_2 this trend is reversed: the C–N double bond in $\mathbf{P_7}$ and $\mathbf{P_8}$ (C5–N1) is longer than the corresponding bond in $\mathbf{P_{10}}$ and $\mathbf{P_{11}}$ (C4–N2), respectively. The C–N single bond in $\mathbf{P_7}$ (C4–N2) is longer than the C5–N1 bond in $\mathbf{P_{10}}$, whereas the C4–N2 bond in $\mathbf{P_8}$ is shorter than the C5–N2 bond. These facts again demon-

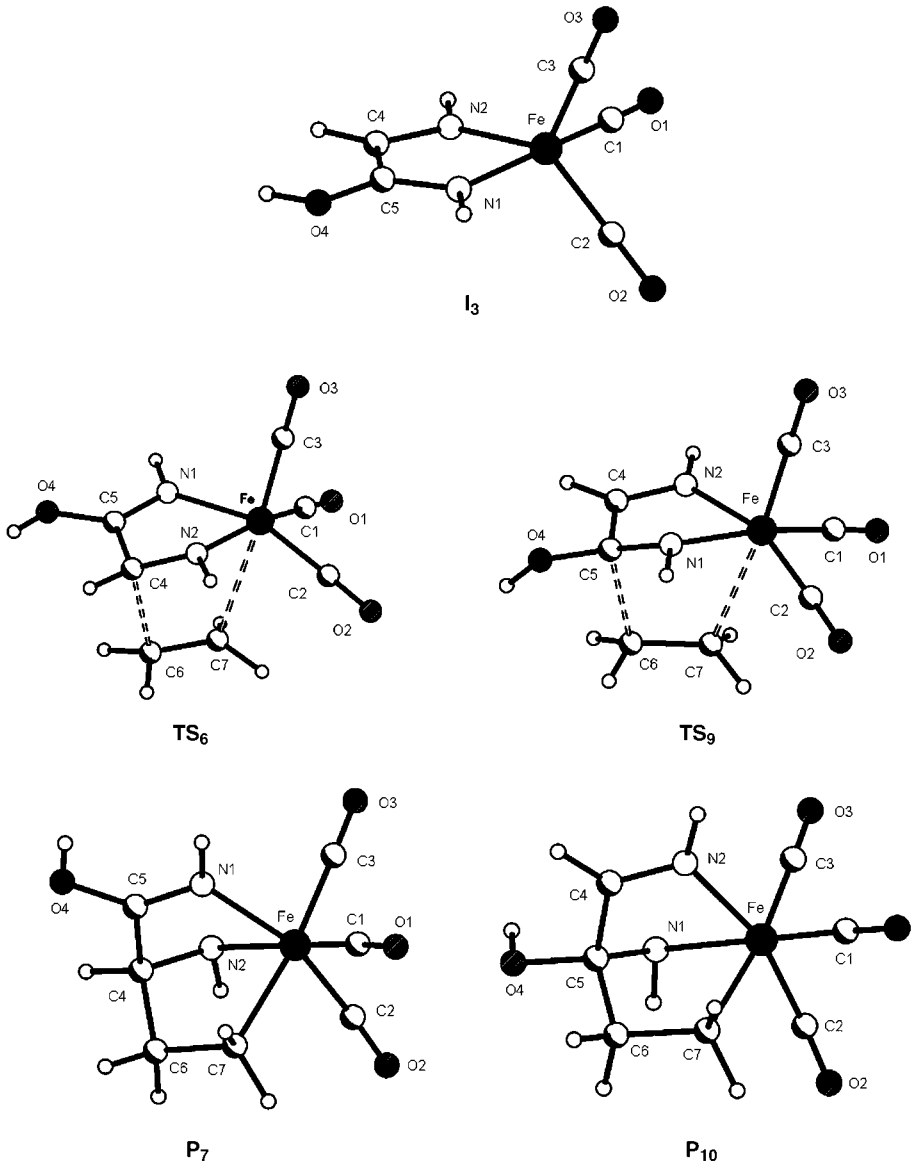

Figure 6. Structures of $\mathbf{I_3}$, $\mathbf{TS_6}$, $\mathbf{TS_9}$, $\mathbf{P_7}$, and $\mathbf{P_{10}}$ optimized at the B3LYP/6–311++G(d,p) level. Bond lengths are given in Table 6.

strate the higher π-donor abilities of a NH_2 substituent, leading to a delocalization of electron density towards the imine moiety.

Table 8 summarizes the calculated total energies of the reactants $\mathbf{I_2}$–$\mathbf{I_4}$, the transition states $\mathbf{TS_5}$–$\mathbf{TS_{10}}$, and the product complexes $\mathbf{P_6}$–$\mathbf{P_{11}}$. Figure 8 shows the energy profiles of the addition of ethylene (**B**) to $\mathbf{I_2}$–$\mathbf{I_4}$. In Table 9 the relative Gibbs free energies of elementary steps leading to the stationary points of the reactions are given.

From Figure 8 and Table 9 it is obvious that for R = F there is no selectivity for the addition of ethylene (**B**) to $\mathbf{I_2}$. The two transition structures represent essentially the same activation barrier. The product in which ethylene is added to the imine group bearing the fluorine substituent ($\mathbf{P_9}$) is just 1.2 kcal mol^{-1} more stable than $\mathbf{P_6}$ relative to the reactants $\mathbf{I_2}$ and **B**.

If a hydroxo group is present in the 2-position of the 1,4-diazabutadiene ($\mathbf{I_3}$), the activation barrier leading to the addition of ethylene to the imine group in the 3-position ($\mathbf{TS_6}$, Scheme 5, Figure 6) is 5.0 kcal mol^{-1} lower than the barrier for the addition of ethylene to the imine bond next to the hydroxo group. The formation of the corresponding products $\mathbf{P_7}$ and $\mathbf{P_{10}}$ is 1.1 kcal mol^{-1} more exothermic for $\mathbf{P_{10}}$. Nevertheless, $\mathbf{P_7}$ is 3.9 kcal mol^{-1} more stable than $\mathbf{P_{10}}$ relative to $\mathbf{I_3}$ and **B**. The differences in the activation energy lead to a regioselective addition of ethylene to $\mathbf{I_3}$ to give $\mathbf{P_7}$.

If an amino group is used as the substituent ($\mathbf{I_4}$, Scheme 5, Figure 7), the addition of ethylene to give $\mathbf{TS_7}$ has an activation barrier 7.6 kcal mol^{-1} lower than that for the formation of $\mathbf{TS_{10}}$. In this case the formation of $\mathbf{P_8}$ from $\mathbf{TS_7}$ is also more exothermic (4.14 kcal mol^{-1}) than the reaction of $\mathbf{TS_{10}}$ to produce $\mathbf{P_{11}}$, leading to an overall stabilization of $\mathbf{P_8}$ over $\mathbf{P_{11}}$ of 11.8 kcal mol^{-1} relative to the reactants $\mathbf{I_4}$ and ethylene. In the reaction of $\mathbf{I_4}$ with ethylene a perfect regioselectivity is therefore expected in generating the product in which ethylene interacts with the imine-carbon atom in the 3-position ($\mathbf{TS_7}$, $\mathbf{P_8}$).

Table 10 shows the NPA charges of selected atoms of $\mathbf{I_2}$–$\mathbf{I_4}$ and the transition states $\mathbf{TS_5}$–$\mathbf{TS_{10}}$. In contrast to the values

Table 8. Calculated total energies E for $\mathbf{I_2}$–$\mathbf{I_4}$, $\mathbf{TS_5}$–$\mathbf{TS_{10}}$ and $\mathbf{P_6}$–$\mathbf{P_{11}}$.[a]

Compound	R	$-E$ [a.u.] [kcal mol^{-1}]	[Nimag][b]	ZPE [kcal mol^{-1}]
$\mathbf{I_2}$	F	1891.3147247	[0]	52.61
$\mathbf{I_3}$	OH	1867.2952703	[0]	60.23
$\mathbf{I_4}$	NH_2	1847.4245624	[0]	68.04
$\mathbf{TS_5}$	F	1969.8888788	[1]	85.77
$\mathbf{TS_6}$	OH	1945.8714572	[1]	93.54
$\mathbf{TS_7}$	NH_2	1926.0015656	[1]	101.20
$\mathbf{TS_8}$	F	1969.8887558	[1]	85.61
$\mathbf{TS_9}$	OH	1945.8629218	[1]	93.16
$\mathbf{TS_{10}}$	NH_2	1925.9893032	[1]	101.14
$\mathbf{P_6}$	F	1969.9172107	[0]	88.04
$\mathbf{P_7}$	OH	1945.9008121	[0]	95.96
$\mathbf{P_8}$	NH_2	1926.0168416	[0]	103.55
$\mathbf{P_9}$	F	1969.918793	[0]	87.83
$\mathbf{P_{10}}$	OH	1945.894105	[0]	95.66
$\mathbf{P_{11}}$	NH_2	1926.0355175	[0]	103.50

[a] All calculations performed at the B3LYP/6–311++G(d,p) level. [b] Number of imaginary frequencies.

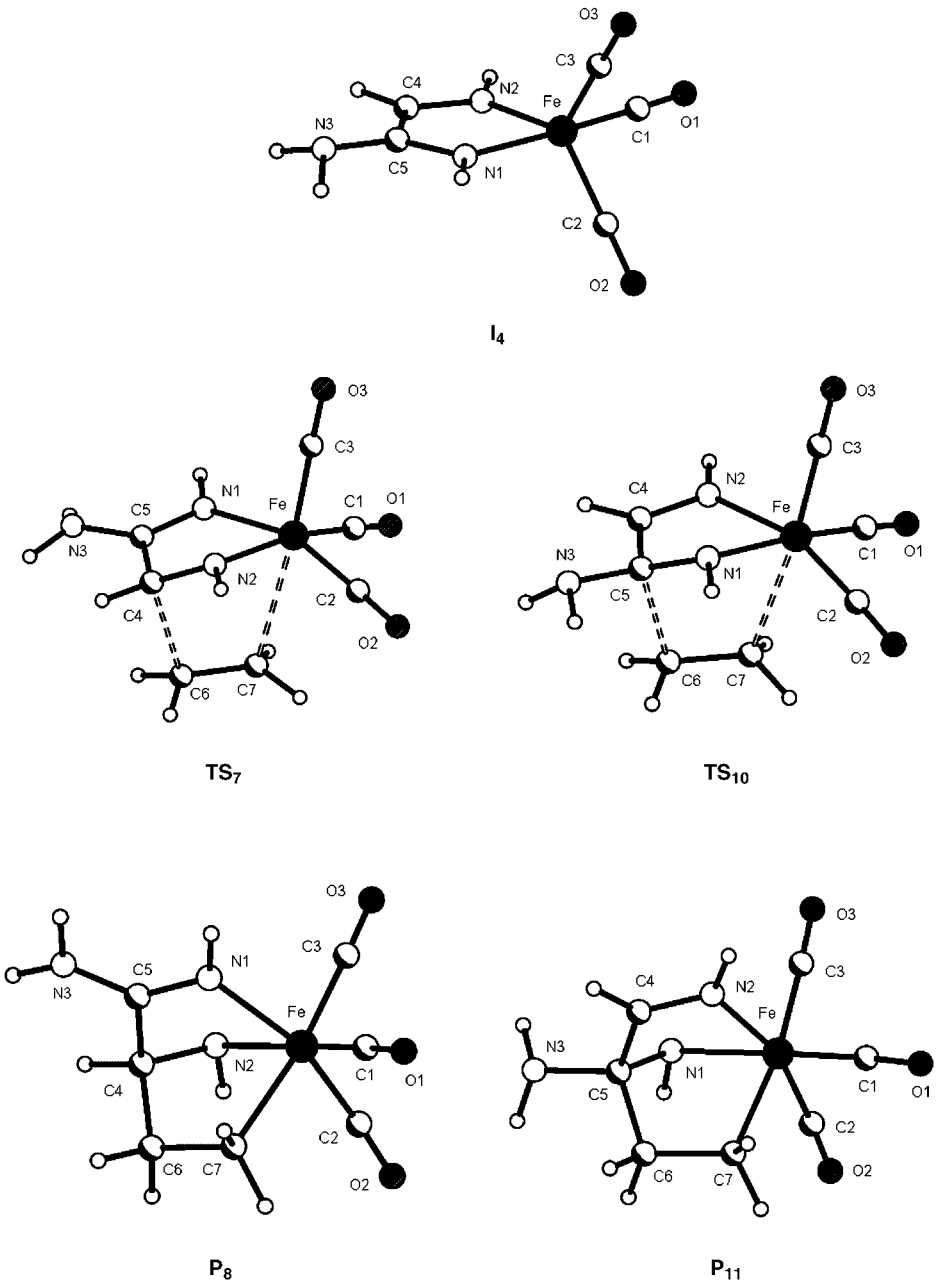

Figure 7. Structures of $\mathbf{I_4}$, $\mathbf{TS_7}$, $\mathbf{TS_{10}}$, $\mathbf{P_8}$, and $\mathbf{P_{11}}$ optimized at the B3LYP/6–311++G(d,p) level. Bond lengths are given in Table 7.

Table 9. Relative Gibbs free energies of elementary steps leading to $\mathbf{TS_5}$–$\mathbf{TS_{10}}$ and $\mathbf{P_6}$–$\mathbf{P_{11}}$.

Elementary step	ΔG [kcal mol^{-1}]
$\mathbf{B+I_2 \rightarrow TS_5}$	27.26
$\mathbf{B+I_2 \rightarrow TS_8}$	27.18
$\mathbf{B+I_3 \rightarrow TS_6}$	26.13
$\mathbf{B+I_3 \rightarrow TS_9}$	31.11
$\mathbf{B+I_4 \rightarrow TS_7}$	25.47
$\mathbf{B+I_4 \rightarrow TS_{10}}$	33.11
$\mathbf{TS_5 \rightarrow P_6}$	−15.51
$\mathbf{TS_8 \rightarrow P_9}$	−16.63
$\mathbf{TS_6 \rightarrow P_7}$	−16.00
$\mathbf{TS_9 \rightarrow P_{10}}$	−17.07
$\mathbf{TS_7 \rightarrow P_8}$	−19.01
$\mathbf{TS_{10} \rightarrow P_{11}}$	−14.87

presented in Table 4 it is obvious here that Coulombic interactions are not the main reason for the regioselectivity in the reaction of $\mathbf{I_3}$ and $\mathbf{I_4}$ compared to $\mathbf{I_2}$. The charge differences between C6 and the imine-carbon atom interacting with ethylene for all substituents is bigger for those transition structures in which an addition of ethylene to the imine group in the 2-position bearing the heteroatom takes place. Taking into account only Coulombic interactions would lead to incorrect predictions in terms of the regioselectivity in the reactions of $\mathbf{I_3}$ and $\mathbf{I_4}$ and would lead to a greatly overestimated value for the regioselectivity in the reaction of $\mathbf{I_2}$. On the other hand, the NPA charges also demonstrate the higher π-donor capability of an amino group compared to the OH and F substituents. The amino-nitrogen atom shows a much higher partial negative charge than O4 and F corresponding with a less positive NPA charge at C5. This means that the amino group is able to effectively establish a delocalized π-electron system with the adjacent imine group by conjugative effects.

Conclusion

From this investigation we conclude that high-level B3LYP/6–311++G(d,p) DFT calculations allow the reliable interpretation and prediction of the subtle substituent effects that are responsible for the regioselectivity of the ethylene addition to substituted [(1,4-diazabutadiene)$Fe(CO)_3$] complexes.

Calculations on related 1,4-diazabutadienes with substituents in the 2-position indicated that the reason for this regioselectivity is not the electronegativity and thus the σ-acceptor ability of the heteroatom, but that this effect is overcompensated for by the π-donor ability of the hetero substituents. The more efficient a directing substituent X, the better it supports—incorporating the adjacent imine moiety—the formation of a delocalized π system, (X)−C=NH with X = H, F, OH, NH_2. In other words, without exception, the ethylene attack will always be directed towards the less stable (X)−C=NR subunit that exhibits the less efficient

Table 10. Calculated partial charges of selected atoms of $\mathbf{I_2}$–$\mathbf{I_4}$ and $\mathbf{TS_5}$–$\mathbf{TS_{10}}$. Calculations performed at the B3LYP/6–311++G(d,p) level.

	Fe	N1	N2	C4	C5	F	C6	C7
$\mathbf{I_2}$	−0.01	−0.73	−0.66	−0.10	0.57	−0.34	–	–
$\mathbf{TS_5}$	−0.09	−0.73	−0.79	−0.07	0.66	−0.34	−0.43	−0.50
$\mathbf{TS_8}$	−0.09	−0.83	−0.66	0.06	0.53	−0.37	−0.44	−0.48
	Fe	N1	N2	C4	C5	O4	C6	C7
$\mathbf{I_3}$	−0.01	−0.72	−0.65	−0.11	0.49	−0.68	–	–
$\mathbf{TS_6}$	−0.09	−0.72	−0.78	−0.07	0.56	−0.67	−0.44	−0.48
$\mathbf{TS_9}$	−0.10	−0.82	−0.66	0.09	0.44	−0.72	−0.46	−0.51
	Fe	N1	N2	C4	C5	N3	C6	C7
$\mathbf{I_4}$	−0.02	−0.72	−0.64	−0.07	0.36	−0.79	–	–
$\mathbf{TS_7}$	−0.09	−0.73	−0.77	−0.03	0.43	−0.79	−0.44	−0.48
$\mathbf{TS_{10}}$	−0.11	−0.83	−0.66	0.11	0.31	−0.82	−0.44	−0.53

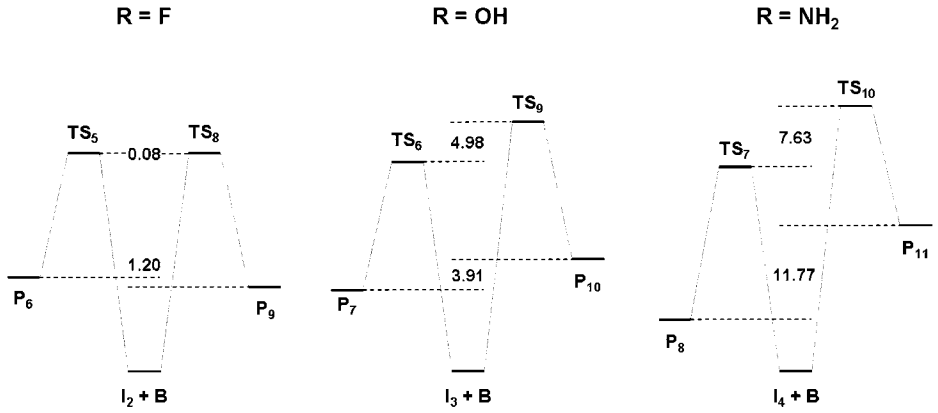

Figure 8. The interaction of ethylene with $\mathbf{I_2}$–$\mathbf{I_4}$. For relative free energies of $\mathbf{I_2}$–$\mathbf{I_4}$, $\mathbf{TS_5}$–$\mathbf{TS_{10}}$, and $\mathbf{P_6}$–$\mathbf{P_{11}}$ see Table 8.

delocalization of π-electron density. If the 2,3-carbon atoms of the 1,4-diazabutadiene are part of an oxazine ring system as in $\mathbf{I_1}$ or in **J** (Scheme 3), the two π systems (O)−C=NH and (N)−C=NH compete. The π system of the (N)−C=NH moiety is obviously better stabilized and thus forces the ethylene attack to the oxygen site. As demonstrated, this pathway demands a lower activation barrier and results in a product that is better stabilized. All our DFT results are in complete agreement with our earlier experimental findings.

[1] a) A. Brandi, F. M. Cordero, F. De Sarlo, R. Gandolfi, A. Rastelli, M. Bagatti, *Tetrahedron* **1992**, *48*, 3323; b) S. E. Denmark, M. Seierstad, B. Herbert, *J. Org. Chem.* **1999**, *64*, 884; c) F. P. Cossio, I. Morao, H. Jiao, P. von Schleyer, *J. Am. Chem. Soc.* **1999**, *121*, 6737; d) A. Rastelli, R. Gandolfi, M. S. Amade, *Adv. Quantum Chem.* **1999**, *36*, 151; e) M. A. Silva, J. M. Goodman, *Tetrahedron* **2002**, *58*, 3667; f) K. Marakchi, O. Kabbaj, N. Komiha, R. Jalal, M. Esseffar, *Theochem* **2003**, *620*, 271; g) G. Wagner, *Chem. Eur. J.* **2003**, *9*, 1503; h) P. Astolfi, P. Bruni, L. Greci, P. Stipa, C. Rizzoli, *Eur. J. Org. Chem.* **2003**, 2626.

[2] a) P. Caramella, G. Cellerino, K. N. Houk, F. M. Albini, C. Santiago, *J. Org. Chem.* **1978**, *43*, 3006; b) T. Hayakawa, K. Araki, S. Shiraishi, *Bull. Chem. Soc. Jpn.* **1984**, *57*, 1643; c) S. Fukuda, A. Kamimura, S. Kanemasa, K. Hori, *Tetrahedron* **2000**, *56*, 1637; d) Y. Hu, K. N. Houk, *Tetrahedron* **2000**, *56*, 8239; e) R. Jalal, M. El Messaoudi, M. Esseffar, *Theochem* **2002**, *580*, 183.

[3] a) R. A. Moss, C. M. Young, L. A. Perez, K. Krogh-Jespersen, *J. Am. Chem. Soc.* **1981**, *103*, 2413; b) R. Sustmann, W. Sicking, *Chem. Ber.* **1987**, *120*, 1653; c) R. Sustmann, W. Sicking, R. Huisgen, *J. Org. Chem.* **1993**, *58*, 82; d) O. Arjona, C. Manzano, J. Plumet, *Heterocycles* **1993**, *35*, 63; e) A. Rastelli, M. Bagatti, R. Gandolfi, *Tetrahedron* **1994**, *50*, 5561; f) L. Nyulaszi, P. Varnai, W. Eisfeld, M. Regitz, *J. Comput. Chem.* **1997**, *18*, 609; g) A. Rastelli, R. Gandolfi, M. S. Amade, *J. Org. Chem.* **1998**, *63*, 7425; h) C. I. Williams, M. A. Whitehead, B. J. Jean-Claude, *Theochem* **1999**, *491*, 103; i) L. T. Nguyen, F. De - Proft, V. L. Dao, M. T. Nguyen, P. Geerlings, *J. Phys. Org. Chem.* **2003**, *16*, 615.

[4] a) B. S. Jursic, Z. Zdravkovski, *Theochem* **1995**, *333*, 209; b) J. J. Klicic, R. A. Friesner, *J. Phys. Chem. A* **1999**, *103*, 1276; c) J. Korchowiec, A. K. Chandra, T. Uchimaru, K. Guminski, *Theochem* **2001**, *572*, 193.

[5] a) K. N. Houk, N. G. Rondan, C. Santiago, C. J. Gallo, R. W. Grandour, G. W. Griffin, *J. Am. Chem. Soc.* **1980**, *102*, 1504; b) F. Bernardi, A. Bottoni, A. Battaglia, G. Distefano, A. Dondoni, *Z. Naturforsch. A* **1980**, *35*, 521; c) M. T. Nguyen, A. F. Hegarty, M. A. McGinn, P. Ruelle, *J. Chem. Soc. Perkin Trans. 2* **1985**, 1991; d) M. T. Nguyen, A. F. Hegarty, *J. Chem. Soc. Perkin Trans. 2* **1985**, 1999; e) M. T. Nguyen, A. F. Hegarty, *J. Chem. Soc. Perkin Trans. 2* **1985**, 2005; f) N. Imai, H. Tokiwa, M. Aono, Y. Terao, Y. Akahori, K. Achiwa, *Heterocycles* **1986**, *24*, 2423; g) N. Imai, H. Tokiwa, Y. Akahori, K. Achiwa, *Chem. Lett.* **1986**, 1113; h) A. Rastelli, M. Bagatti, R. Gandolfi, *J. Am. Chem. Soc.* **1995**, *117*, 4965; i) F. P. Cossio, G. Roa, B. Lecea, J. M. Ugalde, *J. Am. Chem. Soc.* **1995**, *117*, 12306; k) U. Salzner, S. M. Bachrach, *J. Org. Chem.* **1996**, *61*, 237; l) W. M. F. Fabian, R. Janoschek, *J. Am. Chem. Soc.* **1997**, *119*, 4253; m) A. F. Hegarty, S. J. Eustace, N. M. Tynan, N.-N. Pham-Tran, M. T. Nguyen, *J. Chem. Soc. Perkin Trans. 2* **2001**, 1239; n) R. Martinez, H. A. Jiminez-Vasquez, F. Delgado, J. Tamariz, *Tetrahedron* **2003**, *59*, 481; o) H.-T. Chen, J.-J. Ho, *J. Phys. Chem. A* **2003**, *107*, 7643; p) P. Maurin, M. Ibrahim-Ouali, J.-L. Parrain, M. Santelli, *Theochem* **2003**, *637*, 91.

[6] a) S. Pugnaud, D. Masure, J.-C. Halle, P. Chaquin, *J. Org. Chem.* **1997**, *62*, 8687; b) E. V. Babaev, V. V. Simonyan, K. Y. Pasichnichenko, V. M. Nosova, A. V. Kisin, K. Jug, *J. Org. Chem.* **1999**, *64*, 9057.

[7] a) J. M. Fan, Y. Wang, C. Ueng, *Z. Naturforsch. A* **1993**, *48*, 105; b) J. M. Fan, Y. Wang, C. Ueng, *J. Phys. Chem.* **1993**, *97*, 8193.

[8] M. Avalos, R. Babiano, A. Cabanillas, P. Cintas, J. L. Jiminez, J. C. Palacios, *J. Org. Chem.* **1996**, *61*, 7291.

[9] a) J. Haller, B. R. Beno, K. N. Houk, *J. Am. Chem. Soc.* **1998**, *120*, 6468; b) J. O. Morley, D. W. Roberts, S. P. Watson, *J. Chem. Soc. Perkin Trans. 2* **1999**, 1819.

[10] M. F. A. Hendrickx, C. Vinckier, *J. Phys. Chem. A* **2003**, *107*, 7574.

[11] a) M. D. Gordon, P. V. Alston, A. R. Rossi, *J. Am. Chem. Soc.* **1978**, *100*, 5701; b) R. Sustmann, W. Sicking, *J. Am. Chem. Soc.* **1996**, *118*, 12562; c) M. T. Nguyen, A. Van Keer, L. G. Vanquickenborne, *Chem. Ber.* **1997**, *130*, 69.

[12] J. D. Evanseck, J. Mareda, K. N. Houk, *J. Am. Chem. Soc.* **1990**, *112*, 73.

[13] a) S. Yamada, T. Misono, M. Ichikawa, C. Morita, *Tetrahedron* **2001**, *57*, 8939; b) R. Sustmann, W. Sicking, R. Huisgen, *J. Am. Chem. Soc.* **2003**, *125*, 14425.
[14] a) V. V. Penkovskii, V. I. Kharchenko, L. N. Alekseiko, *Teor. Eksp. Khim.* **1991**, *27*, 462; b) M. T. Nguyen, L. Landuyt, L. G. Vanquickenborne, *J. Org. Chem.* **1993**, *58*, 2817; c) V. Penkovsky, V. Kharchenko, L. Alexeiko, *Phosphorus SulfurSilicon Relat. Elem.* **1993**, 77, 81.
[15] a) A. Göbel, W. Imhof, *Chem. Commun.* **2001**, 593; b) A. Göbel, W. Imhof, *J. Mol. Catal. A* **2003**, *197*, 15.
[16] W. Imhof, E. Anders, A. Göbel, H. Görls, *Chem. Eur. J.* **2003**, *9*, 1166.
[17] W.-M. Dai, C. W. Lau, S. H. Chung, Y. D. Wu, *J. Org. Chem.* **1995**, *60*, 8128.
[18] A. Venturini, J. Joglar, S. Fustero, J. Gonzalez, *J. Org. Chem.* **1997**, *62*, 3919.
[19] A. B. Mandal, A. Gomez, G. Trujillo, F. Mendez, H. A. Jiminez, M. de Jesus Rosales, R. Martinez, F. Delgado, J. Tamariz, *J. Org. Chem.* **1997**, *62*, 4105.
[20] J. A. Varela, L. Castedo, M. Maestro, J. Mahia, C. Saa, *Chem. Eur. J.* **2001**, *7*, 5203.
[21] a) R. Beckhaus, J. Sang, T. Wagner, B. Ganter, *Organometallics* **1996**, *15*, 1176; b) R. Beckhaus, J. Sang, U. Englert, *Organometallics* **1996**, *15*, 4731; c) R. Beckhaus, J. Sang, T. Wagner, U. Böhme, *J. Chem. Soc. Dalton Trans.* **1997**, 2249.
[22] Gaussian 98, Revision A11, M. J. Frisch, G. W. Trucks, H. B. Schlegel, G. E. Scuseria, M. A. Robb, J. R. Cheeseman, V. G. Zakrzewski, J. A. Montgomery, Jr., R. E. Stratmann, J. C. Burant, S. Dapprich, J. M. Millam, A. D. Daniels, K. N. Kudin, M. C. Strain, O. Farkas, J. Tomasi, V. Barone, M. Cossi, R. Cammi, B. Mennucci, C. Pomelli, C. Adamo, S. Clifford, J. Ochterski, G. A. Petersson, P. Y. Ayala, Q. Cui, K. Morokuma, D. K. Malick, A. D. Rabuck, K. Raghavachari, J. B. Foresman, J. Cioslowski, J. V. Ortiz, B. B. Stefanov, G. Liu, A. Liashenko, P. Piskorz, I. Komaromi, R. Gomperts, R. L. Martin, D. J. Fox, T. Keith, M. A. Al-Laham, C. Y. Peng, A. Nanayakkara, C. Gonzalez, M. Challacombe, P. M. W. Gill, B. Johnson, W. Chen, M. W. Wong, J. L. Andres, M. Head-Gordon, E. S. Replogle, J. A. Pople, Gaussian, Inc., Pittsburgh PA, **2002**.
[23] A. D. Becke, *J. Chem. Phys.* **1993**, *98*, 5648.
[24] C. Lee, W. Yang, R. G. Parr, *Phys. Rev. B* **1988**, *37*, 785.
[25] R. S. Grev, H. F. Schaefer III, *J. Chem. Phys.* **1989**, *91*, 7305.
[26] a) A. D. Becke, *J. Chem. Phys.* **1992**, *97*, 9173; b) P. E. M. Siegbahn, M. R. A. Bomberg, *Chem. Rev.* **2000**, *100*, 421.
[27] P. Pulay in *Ab initio Methods in Quantum Chemistry* (Ed.: K. P. Lawley), Wiley, New York, **1987**, p. 241.
[28] For a brief introduction see a) J. W. Ochterski, Gaussian Inc. **1999**, 1; b) J. W. Ochterski, Gaussian Inc. **2000**, 1; c) P. Y. Ayala, H. B. Schlegel, *J. Chem. Phys.* **1997**, *108*, 2314.
[29] a) A. E. Reed, F. J. Weinhold, *J. Chem. Phys.* **1983**, *78*, 4066; b) A. E. Reed, R. B. Weinstock, F. J. Weinhold, *J. Chem. Phys.* **1985**, *83*, 735.

Received: March 4, 2004
Published online: October 7, 2004

